Title

Trace Levels of Copper in Carbon Materials Show Significant Electrochemical CO2 Reduction Activity

Journal

ACS Catalysis, 6(1)

ISSN

2155-5435

Authors

Lum, Yanwei
Kwon, Youngkook
Lobaccaro, Peter
et al.

Publication Date

2016-01-04

DOI

10.1021/acscatal.5b02399

Peer reviewed

ACS Catalysis

Research Article

pubs.acs.org/acscatalysis

Trace Levels of Copper in Carbon Materials Show Significant Electrochemical CO_2 Reduction Activity

Yanwei Lum,[†,‡,∥,#] Youngkook Kwon,[†,‡,#] Peter Lobaccaro,[†,‡,⊥] Le Chen,[†,‡] Ezra Lee Clark,[†,‡,⊥] Alexis T. Bell,[*,†,§,⊥] and Joel W. Ager[*,†,‡,∥]

[†]Joint Center for Artificial Photosynthesis, [‡]Materials Sciences Division, and [§]Chemical Sciences Division, Lawrence Berkeley National Laboratory, Berkeley, California 94720, United States

[∥]Department of Materials Science and Engineering and [⊥]Department of Chemical and Biomolecular Engineering, University of California, Berkeley, California 94720, United States

Supporting Information

ABSTRACT: Carbon materials are frequently used as supports for electrocatalysts because they are conductive and have high surface area. However, recent studies have shown that these materials can contain significant levels of metallic impurities that can dramatically alter their electrochemical properties. Here, the electrocatalytic activity of pure graphite (PG), graphene oxide (GO), and carbon nanotubes (CNT) dispersed on glassy carbon (GC) are investigated for the electrochemical CO_2 reduction reaction (CO2RR) in aqueous solution. It was observed that GO and CNT dispersed on GC all exhibit significant electrochemical activity that can be ascribed to impurities of Ni, Fe, Mn, and Cu. The level of Cu in GO can be particularly high and is the cause for the appearance of methane in the products produced over this material when it is used for the CO2RR. Washing these supports in ultrapure nitric acid is effective in removing the metal impurities and results in a reduction in the electrochemical activity of these forms of carbon. In particular, for GO, nearly all of the catalytically relevant metals can be removed. Electrochemical deposition of Cu on GO and PG supported on GC, and on GC itself, increased both the electrochemical activity of these materials and the production of methane via the CO2RR. Particularly high rates of methane formation per unit of Cu mass were obtained for Cu electrodeposited on GO and PG supported on GC. We suggest that this high activity may be due to the preferential deposition of Cu onto defects present in the graphene sheets comprising these materials.

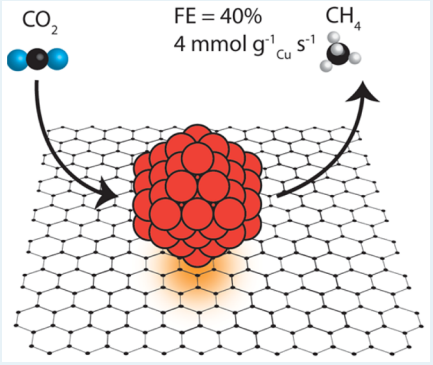

KEYWORDS: *CO_2 electroreduction, Faradaic efficiency, electrocatalytic activity, graphene oxide, carbon nanotubes*

INTRODUCTION

Electrochemical reduction of carbon dioxide is an attractive option for converting electrical power produced by solar radiation and wind into sustainable fuels.[1−8] To meet this objective, electrocatalysts are required that have high energy conversion efficiency, selectivity to liquid fuels, and long operational lifetimes.[9−12] Prior research has shown that Cu is the only metallic electrocatalyst that is active for producing hydrocarbons via the CO_2 reduction reaction (CO2RR) in aqueous solution and which exhibits appreciable selectivity to hydrocarbons and alcohols.[1,9,13] However, studies conducted with polycrystalline Cu have demonstrated that, in order to achieve significant CO2RR activity (e.g., current densities >5 mA cm^{-2}), overpotentials in excess of 1 V are required, which contributes to a low overall energy conversion efficiency for the process.[9,14] To overcome this limitation, efforts have been undertaken to disperse Cu nanoparticles on carbon supports, because this enables the amount of active catalyst area per unit of electrode to be increased. Such supports are also attractive because they are electrically conductive and can be made with high surface area.[15]

It is notable that several investigators have found carbon-based materials to be active for the CO2RR even in the absence of added metal. For example, Kumar et al. have reported that nitrogen-doped carbon nanofibers produce CO with high selectivity at an overpotential of 0.17 V,[16] and Nakata et al. have noted that boron-doped diamond electrocatalysts produce formaldehyde with a Faradaic efficiency of up to 74%.[17] Very recently, Zhang et al.[18] and Wu et al.[19] reported that nitrogen-doped carbon nanotubes can produce formic acid and CO, respectively, with Faradaic efficiencies of over 80%.

However, the question arises as to whether or not the carbon-based materials used in these studies contain metal impurities. Recent work has shown that trace metal impurities present on carbon supports can substantially influence their electrochemical activity.[20] For example, it has been shown that much of the apparent activity of carbon nanotubes for hydrazine oxidation is actually due to metal impurities.[21]

Received: July 23, 2015
Revised: November 20, 2015
Published: November 23, 2015

DOI: 10.1021/acscatal.5b02399
ACS Catal. 2016, 6, 202−209

Moreover, the metal impurities can persist in carbon nanotubes despite efforts to remove them via dissolution in strong acid and rinsing.[22,23] While in the case of nanotubes it could be thought that the metal contaminants are on the interior of the tubes, graphene supports have also been reported to have detectable levels of metal contaminants.[24−26] Notably, it has been found that copper is a major impurity of graphene oxide materials.[24,26] Also, Wuttig and Surendranath have recently shown that trace levels of metals in the electrolyte can be difficult to remove and can have a major impact on electrode selectivity.[27] Certainly, the presence of metal impurities in the electrode and in the electrolyte combined with the difficulty in removing them creates challenges for producing "metal-free" supports. For example, in a recent study of the hydrogen evolution reaction on carbon supports, Dong et al.[28] found that metals from the counter electrode can deposit in situ on the working electrode, significantly enhancing its activity. Consequently, it becomes important to understand the role that impurities such as Fe, Ni, and Cu might have on the activity of carbon supports for the CO2RR, a subject which to the best of our knowledge has not been previously investigated.

EXPERIMENTAL SECTION

Materials. Graphene oxide (sheets), sodium carbonate (≥99.9999% metals basis), potassium chloride (99.999% metals basis), Cu acetylacetonate (99.99%), oleylamine (70%), Nafion solution (10 wt % dispersion in water), and ethanol (absolute ≥99.5%) were purchased from Sigma-Aldrich. Graphene oxide was also purchased from ACS Materials LLC and Graphene Supermarket, and reduced graphene oxide was purchased from Sigma-Aldrich. Potassium ferricyanide (≥99%) was purchased from Fisher Chemical. Glassy-carbon plate (type 2, 2 mm thick), glassy-carbon rod (type 2, 5 mm diameter), graphite powder (≥99.9999% metals basis), and copper(II) sulfate hydrate (≥99.999% metals basis) were purchased from Alfa Aesar. Multiwalled carbon nanotubes (20−30 nm diameter, 0.5−2 μm length, >95% purity) were purchased from Nanostructured & Amorphous Materials, Inc. Water-based alumina fine polishing suspension (0.05 μm) and polishing cloth (Alpha-A, 8 in.) were purchased from Ted Pella, Inc. ACS reagent grade nitric acid was purchased from EMD Millipore. High-purity nitric acid (Aristar Ultra) was purchased from BDH Chemicals. Carbon dioxide (99.995%), nitrogen (99.999%), helium (99.999%), and hydrogen (99.999%) were purchased from Praxair. Hydrogen, helium, nitrogen, and carbon dioxide gas purifiers were purchased from Valco Instruments Co. Inc. All chemicals were used without further purification. Electrolyte solutions were prepared with 18.2 MΩ deionized water from a Millipore system.

Preparation of Cu Nanoparticles. Cu nanoparticles were synthesized by the thermal decomposition of Cu acetylacetonate ($Cu(acac)_2$) in oleylamine following the method of Uk Son et al.[29] In brief, 10 mL of oleylamine was heated to 130 °C in a 50 mL three-neck flask equipped with a condenser and stirrer bar under nitrogen for 30 min and then cooled to room temperature. Next, 100 mg of $Cu(acac)_2$ was added to the oleylamine. The solution was slowly heated to 230 °C and kept at this temperature for 6 h, producing a red colloidal solution. After it was cooled to room temperature, the colloidal solution was transferred to a mixture of toluene and ethanol, after which the solution turned green, indicating that Cu nanoparticles were oxidized to Cu oxide. Cu nanoparticles were collected by centrifuging at 8000 rpm for 20 min and decanting the solvent. The nanoparticles were then resuspended in toluene and ethanol, re-collected by centrifuging, and finally dried under vacuum overnight.

Nitric Acid Washing Procedure. For this procedure, 10 mL of concentrated nitric acid was added to a small amount of each of the carbon materials (~20 mg) in a centrifuge tube. To ensure sufficient dispersion of the materials, the mixture was shaken vigorously and then sonicated for 3 h. The resulting dispersion was then filtered, and the filtrate was collected for inductively coupled plasma mass spectrometry (ICP-MS) analysis. The carbon materials left behind as residue were then rinsed briefly with more acid and finally with deionized water until the pH of the filtrate became neutral. The carbon materials were then dried under vacuum overnight. The same procedure was used for washing with both ACS-grade and high-purity nitric acid.

ICP-MS Analysis. For ICP-MS analysis, samples were first diluted with 2% ultrapure nitric acid and then analyzed on an Elan DRC II ICP-MS instrument (PerkinElmer) using a PFA nebulizer and spray chamber at 1500 W rf power. Generally, the most abundant isotopes of analytes were chosen during analysis. In addition, ammonia and oxygen were used as reaction gases to remove interferences for Cr and Fe analysis. Elements that were evaluated include Cr, Mn, Fe, Ni, Co, Cu, Zn, Ga, Ag, Pb, Bi, and Sn.

Materials Characterization. X-ray photoelectron spectroscopy (XPS) was performed using a Kratos Axis Ultra DLD system using a monochromatized Al Kα source ($h\nu$ = 1486.6 eV). A takeoff angle of 0° relative to the surface normal was used to sample the maximum surface depth. The morphology of the carbon materials coated on glassy carbon before and after Cu deposition was characterized using a FEI Quanta 200 FEG SEM instrument. The morphology of Cu(0.1)GO cleaned/GC and Cu nanoparticles was characterized using transmission electron microscopy (TEM) on a modified Philips CM300FEG/UT instrument, with a field-emission electron source and an ultratwin objective lens with low spherical aberration and a point-to-point resolution of 1.7 Å.

Determination of Electrochemically Active Surface Area (EASA). To determine the EASA of the electrodes, cyclic voltammetry using the ferri-/ferrocyanide redox couple ($[Fe(CN)_6]^{3-/4-}$) was employed. In brief, carbon materials were drop-cast and supported on a prepolished glassy-carbon plate as the working electrode. Cyclic voltammetry was carried out in a nitrogen-purged 5 mM $K_3Fe(CN)_6$/0.1 M KCl solution with platinum gauze as the counter electrode. EASA values were calculated using the Randles−Sevcik equation:[18]

$$I_p = (2.69 \times 10^5) n^{3/2} A D^{1/2} C \nu^{1/2}$$

where I_p is the peak current (A), n = 1, D is the diffusion coefficient ($cm^2\ s^{-1}$), ν is the scan rate ($V\ s^{-1}$), C is the concentration of potassium ferricyanide ($mol\ cm^{-3}$), and A is the electrode area (cm^2).

Electrode Preparation. The glassy-carbon plate was first cut into 2.2 cm × 2.2 cm dimensions and cleaned by sonicating in acetone followed by isopropyl alcohol and finally by deionized water. The glassy-carbon plate was then mechanically polished using an alumina suspension up to 0.05 μm on a polishing cloth. To remove any possible metallic impurities, the glassy-carbon plates were soaked in 1 M high-purity nitric acid for 2 h and rinsed with deionized water. Before every

DOI: 10.1021/acscatal.5b02399
ACS Catal. 2016, 6, 202−209

experiment, only the nitric acid treatment and mechanical polishing were carried out on the glassy carbon.

Carbon materials were first prepared by dispersing them in ethanol. A 1 mL portion of ethanol and 5 μL of Nafion binder solution were added for every 1 mg of material. Nafion acts only as a binder for mechanical integrity and is not expected to have a major effect on the activity of the carbon materials under electrolysis conditions. The resulting mixture was then sonicated for 30 min to ensure adequate dispersion. For electrochemical testing, 30 μL of the mixture was drop-cast onto a glassy-carbon plate and spin-coating at 1000 rpm was carried out to ensure evenness. An additional 30 μL mixture was coated on top of the initial layer followed by a final layer using 20 μL. Therefore, in total, 80 μL of the mixture was effectively deposited onto the glassy-carbon substrates. To take into account the losses from spin-coating, separate electrodes were prepared by drop-casting the carbon materials onto glassy carbon, which were then allowed to dry (see the Supporting Information). The EASA values of these electrodes were probed using the ferri-/ferrocyanide redox couple and compared to those of the spin-coated electrodes to determine the actual mass loading of carbon material on the glassy-carbon plate (Table S1 in the Supporting Information).

Cu nanoparticles were drop-cast and spin-coated onto a glassy-carbon plate with a suspension containing 71.4 μg of Cu in 1 mL of ethanol using an identical method. To take into account losses of material during spin-coating, three samples were made using this procedure, and subsequently each of them were soaked into 1 M nitric acid to dissolve the Cu nanoparticles. The resultant solution was then analyzed using ICP-MS to determine the Cu concentration, which then can be directly correlated to the actual mass loading of Cu on the glassy-carbon plate. It was determined that, on average, 3.35 μg out of the 5.71 μg of Cu nanoparticles was successfully deposited each time. For electrolysis, only 1 cm^2 of the glassy-carbon substrate was exposed to electrolyte. Therefore, assuming an even dispersion of nanoparticles, it was determined that 0.692 μg of Cu nanoparticles was present in 1 cm^2. To obtain a lower loading of nanoparticles, the same Cu nanoparticle suspension was diluted by a factor of 2 with ethanol to obtain 0.346 μg of Cu on GC (in 1 cm^2).

Preparation of Electrolytes. To make a 0.1 M $NaHCO_3$ solution, a 0.05 M Na_2CO_3 solution was bubbled for 1 h with CO_2. Pre-electrolysis of the electrolyte was also carried out to remove any metallic contaminants that might be present.[1] For this procedure, platinum gauze was used as the working electrode in a two-electrode configuration and a cathodic potential of −2 V was applied for 24 h. Another piece of platinum gauze was used as the counter electrode. Before electrolysis, the electrolyte was bubbled with CO_2 until the pH of the solution reached a value of 6.8 to ensure that the solution was saturated with CO_2.[9] To prepare Cu-spiked electrolytes, appropriate amounts of Cu(II) sulfate hydrate were added to make 0.1 M $NaHCO_3$ solutions with Cu concentrations of 0.01, 0.1, 1, and 2 ppm.

Electrochemical Measurements. Electrochemical measurements were carried out using a Biologic SP-300 potentiostat. Ambient-pressure CO_2 electrolysis was carried out in a custom-made gastight electrochemical cell made of polycarbonate and fitted with Buna-N O-rings. The configuration of the electrochemical cell was such that the working electrode sat parallel with respect to the counter electrode (platinum foil) to ensure a uniform potential distribution across the surface. The geometric surface area for both of the electrodes was 1 cm^2. A Selemion AMV anion exchange membrane was used to separate the anodic and cathodic compartments. Each of the compartments in this cell contained a small volume of electrolyte (0.5 mL each) to concentrate liquid products and therefore increase detection limits. The headspace of the cathodic compartment was approximately 0.3 mL.

Before CO_2 electrolysis was conducted, the electrolyte in the cathodic compartments was purged with CO_2 for at least 15 min. During electrolysis, CO_2 was constantly bubbled through the electrolyte at a flow rate of 5 sccm to prevent depletion of CO_2 in the electrolyte and to allow continuous analysis of gaseous products via a gas chromatograph. The flow rate of CO_2 was controlled with a mass flow controller (Alicat Scientific), and the gas was first humidified with water by passing it through a bubbler to minimize evaporation of electrolyte. For all experiments, platinum foil was used as the counter electrode and Ag/AgCl electrode (leak free series) from Innovative Instruments, Inc. was used as the reference. Data were converted to the RHE reference scale using the equation

$$E\ (\text{vs RHE}) = E\ (\text{vs Ag/AgCl}) + 0.197\ \text{V} + 0.0591\text{pH}$$

where the pH was 6.8. To ensure the accuracy of the reference electrodes, calibration was done with a homemade reversible hydrogen electrode.

Product Analysis. For gas product analysis, a gas chromatograph (SRI instruments) equipped with a packed HaySep D column and a packed MolSieve 5A column was used. For detection of gas products, a flame ionization detector (FID) with a methanizer was used to detect hydrocarbons (CO, CH_4, C_2H_4, and C_2H_6) with helium as the carrier gas. A thermal conductivity detector (TCD) was used to detect hydrogen with nitrogen as the carrier gas. Calibration of the gas chromatograph was done using calibration gas from Praxair (UN 1956) with 0.1% CO, 0.099% ethane, 0.099% ethylene, 0.1% hydrogen, and 0.1% ethane balanced in helium. Additional calibration points were achieved by dilution of the calibration gas with appropriate flow rates of helium gas. To further calibrate the hydrogen peak, calibration gas from Praxair (UN 1956) containing 500 ppm of hydrogen and the balance as nitrogen was used. After it passed through the cell, the CO_2 was allowed to flow directly into the gas sampling loop of the GC for online gaseous product analysis, which was carried out every 30 min. For all experiments, electrolysis was allowed to proceed for 2 h with gas analysis done at 25, 55, 85, and 115 min.

The liquid products were collected from the cathode and anode chambers after electrolysis and analyzed by high-performance liquid chromatography (HPLC) on an UltiMate 3000 instrument from Thermo Scientific. Vials with the collected samples were placed in an autosampler holder, and 10 μL of sample was injected into the column. The column used was an Aminex HPX 87-H (Bio-Rad), and diluted sulfuric acid (1 mM) was used as the eluent. The temperature of the column was maintained at 60 °C in a column oven, and the separated compounds were detected with a refractive index detector (RID). The expected products of the CO2RR were analyzed as well by HPLC to produce a standard calibration curve at 60 °C (i.e., formate, acetate, ethylene glycol, ethanol, and *n*-propanol).

DOI: 10.1021/acscatal.5b02399
ACS Catal. 2016, 6, 202−209

RESULTS AND DISCUSSION

Analysis of Carbon Materials for Trace Metals. The GC electrode and the three carbon supports were characterized by X-ray photoelectron spectroscopy (XPS) to determine if any metallic impurities were present in detectable quantities (Figure S1 in the Supporting Information). While there have been reports that XPS can be used to detect metal impurities on carbon supports,[18,21] we did not detect the presence of any metallic impurities, leading us to conclude that XPS is not sufficiently sensitive to detect very small amounts of impurities that may be highly catalytically active.

As a more sensitive alternative, a method was developed for leaching metallic impurities from the carbon material and then analyzing the leachate with inductively coupled plasma mass spectrometry (ICP-MS), a technique which has detection limits in parts per trillion. A fixed amount of pure graphite (PG), carbon nanotubes (CNT), or graphene oxide (GO) and was sonicated for 3 h in ultrahigh-purity concentrated nitric acid. The material was then filtered, and the filtrate was analyzed using ICP-MS. The amount (in ppm by mass) of each impurity removed from the carbon support was calculated from its concentration in the filtrate. The results shown in Table 1

Table 1. Calculated Impurity Concentrations of Metallic Impurities in the as-Received Carbon Materials Based on Extraction with Ultrapure Nitric Acid and ICP-MS Analysis[a]

	calcd impurity concentration (ppm/w)			
sample	Mn	Fe	Ni	Cu
PG	ND	3.71	ND	0.01
PG wash 2	ND	ND	0.992	ND
GO	3600	50.8	3.46	119
GO wash 2	182	2.32	1.00	1.09
CNT	10.7	84.9	1150	3.00
CNT wash 2	ND	3.94	60.2	ND

[a]See Table S2 in the Supporting Information for more detailed information. Abbreviations: PG, high-purity graphite; GO, graphene oxide; CNT, carbon nanotubes; ND, not detected.

demonstrate that significant quantities of the first-row transition metals Mn, Fe, Ni, and Cu are present in GO, PG, and CNT. Other impurities at lower levels were also detected and are reported in Table S2 in the Supporting Information. To assess the effectiveness of the first nitric acid wash in removing impurities, a second nitric acid wash was carried out. As shown in Table 1, much lower impurity levels were found in the second wash relative to the first wash. We should note that prior work with acid washing has shown that is difficult to remove all impurities from carbon materials, especially CNTs, due to intercalation of the metals within the graphitic structure or sheathing within graphene sheets.[22,24,25] Although it is difficult to rule out such a scenario from occurring here, we believe the procedure used here provides a reliable estimate of the type and concentration of impurities in the as-received carbon materials.

Table 1 demonstrates that GO contains the highest level of impurities: Mn, ~3800 ppm; Cu, ~120 ppm; Fe, ~53 ppm; Ni, ~4 ppm. CNT contains lower levels of impurities: Ni, ~1200 ppm; Fe, ~90 ppm; Mn, ~11 ppm; Cu, 3 ppm. The cleanest material is PG, which contains only ~4 ppm of Fe and 0.01 ppm of Cu.

CO2RR Activity of Unmodified Materials. The CO2RR was performed at a cathodic potential of −1.3 V (vs RHE) for 2 h in 0.1 M $NaHCO_3$. The product distributions and current densities for each sample are summarized in Figure 1. The GC

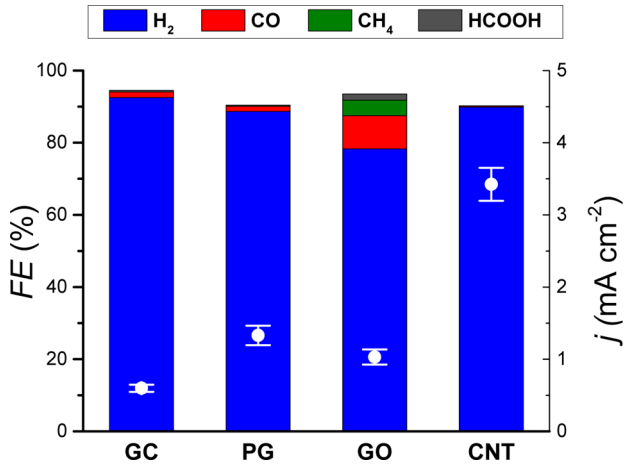

Figure 1. Faradaic efficiencies (FE, shown as bars, left-hand axis) and current densities (open white circles with error bars, right-hand axis) of a glassy-carbon electrode (GC) and as-received carbon supports dispersed on glassy-carbon electrodes: high purity graphite (PG), graphene oxide (GO), and carbon nanotubes (CNT). Electrolysis was carried out at −1.3 V vs RHE for 2 h in 0.1 M $NaHCO_3$ solution. See Table S3 in the Supporting Information for detailed product distribution information.

electrode shows low activity and produces mainly H_2 and very small amounts of CO and HCOOH. PG dispersed on GC (PG/GC) is somewhat more active, but the distribution of products is similar to that seen for GC alone. GO dispersed on GC (GO/GC) produces methane with a Faradaic efficiency (FE) of 4.3%. CNT dispersed on GC (CNT/GC) has the highest current density, 3.2 mA cm^{-2}, and a FE of nearly 100% for H_2.

The activity of GO/GC for methane production strongly implies that the formation of methane is due to the small amounts of Cu present as impurities in GO. The CNT/GC sample exhibited the highest current density and nearly 100% selectivity for H_2 production. The high activity of this sample is likely due to presence of nickel impurities, since Ni is known to be an active catalyst for the hydrogen evolution reaction (HER).[30,31] GC and PG/GC show high FEs for hydrogen but current densities lower than those observed for CNT/GC. The low activity of these samples is very likely due to their low level of contamination by metallic impurities. The somewhat higher current density of PG/GC in comparison to that of GC can be partially attributed to its higher electroactive surface area (Table S1 in the Supporting Information).

On the basis of the measured loading of GO (Table S1 in the Supporting Information) on GC and the Cu concentration in GO, we estimate 1.07 ng cm^{-2} of Cu to be present on GO/GC. GO also contains other metal impurities, in particular Mn and Fe. Under CO2RR conditions, Fe is known to produce H_2 with >90% Faradaic efficiency[1,32] and the case is similar for Mn.[33,34] These impurities likely compete with Cu, which explains why, in addition to methane, GO/GC produces ~80% hydrogen. Also, GO/GC was observed to produce a significant amount of CO, while both GC and PG/GC produced a small amount of CO.

DOI: 10.1021/acscatal.5b02399
ACS Catal. 2016, 6, 202−209

CO2RR Activity of Materials Washed with High-Purity Nitric Acid. The CO2RR activities of PG/GC, GO/GC, and CNT/GC determined after washing in ultrapure nitric acid are shown in Figure 2. The methane formation observed for the as-received GO/GC is clearly eliminated by the washing procedure. Concomitantly, the current density for GO/GC and CNT/GC decreased to 1 mA cm^{-2} or lower. For GO/GC, we attribute the elimination of methane formation to the removal of the Cu impurities in the GO. The data in Table 1 show that, after two washings, the Cu concentration in GO is reduced by an order of magnitude. After washing, PG/GC, CNT/GC, and GO/GC generate predominantly hydrogen together with small amounts of CO and HCOOH. The observed formation of CO and HCOOH might be due to the intrinsic electrocatalytic property of the carbon materials, which might have been previously concealed due to the presence of metallic impurities. It is also possible that the nitric acid treatment induces defects into the carbon structure, which might be active for CO and HCOOH generation. It is conceivable that CO-producing metal impurity remains on the GO after the washing procedure, but we consider this less likely, as electrodes made with washed GO from different sources produce similar current densities and product distributions (see below). Finally, it is important to note that, for cleaning the carbon materials, the purity of the acid used is of high importance. For example, when reagent grade nitric acid was used for cleaning, it was found that the CO2RR activity of GO, CNT, and PG actually increased (see Figure S6 and Table S9 in the Supporting Information).

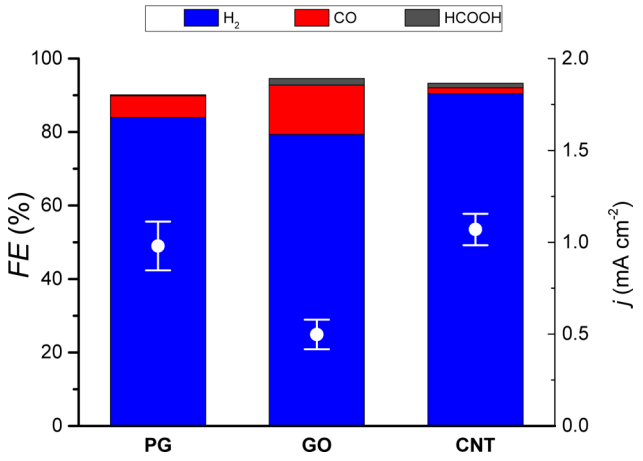

Figure 2. Faradaic efficiencies (FE, shown as bars, left-hand axis) and current densities (open white circles with error bars, right-hand axis) of high-purity nitric acid washed carbon supports dispersed on glassy-carbon electrodes. Treatment with high-purity nitric acid removes any methane formation. Electrolysis was carried out at −1.3 V vs RHE for 2 h in 0.1 M $NaHCO_3$ solution. See Table S4 in the Supporting Information for detailed product distributions.

Batch to Batch Variability of Graphene Oxide. Since it is known that the metallic impurities present in graphene oxide can vary depending on the source of carbon and the synthesis method,[26] we obtained these materials from three additional sources for testing (see the Supporting Information for details). We identified two batches of graphene oxide that showed observable methane production during the CO2RR and one batch that showed >20% selectivity to formic acid (Figure S4a and Table S6 in the Supporting Information). ICP-MS analysis of the leachate following the cleaning procedure found the presence of a variety of metallic impurities, principally Mn, Fe, and Cu (Figure S3 and Table S5 in the Supporting Information). After the cleaning procedure, methane production was eliminated and the current densities of all the graphene oxide materials decreased to similar values, 0.4−0.5 mA cm^{-2} (Figure S4b and Table S7 in the Supporting Information). The product distributions were also similar, with all samples producing predominantly H_2 but with some amounts of CO (5−13%) and HCOOH (0.8−2%).

Electrocatalytic Activity as a Function of Cu Content. The results presented above indicate that the formation of methane during the CO2RR from as-received GO/GC can be attributed to the presence of Cu impurities in the GO. While the Cu content of this catalyst is only ∼120 ppm, its mass activity for methane production at an applied voltage of −1.3 V vs RHE is very high, 54.67 mmol g^{-1} s^{-1}. This observation suggests that very low loadings of Cu on carbon supports may exhibit high activities. To explore this idea, Cu was added intentionally in ppm quantities (0.01−2 ppm) to the sodium bicarbonate electrolyte. Then CO2RR experiments were carried out with the acid-washed GO/GC and as-received PG/GC.

Table 2. Comparison of the Mass Activity per Unit Mass of Cu to Methane Formation of Graphene-Supported Cu versus Cu Nanoparticles on Glassy Carbon[a]

sample/electrolyte	partial current density to methane (mA cm^{-2})	total amount of Cu (μg)	methane activity (mmol g^{-1} s^{-1})	particle size (nm)
GO as received/GC	0.0452	1.07×10^{-3}[b]	54.67	
Cu(0.01)GO cleaned/GC	0.005	1.93×10^{-3}	3.50	
Cu(0.1)GO cleaned/GC	0.201	4.23×10^{-2}	6.17	
Cu(1)GO cleaned/GC	1.453	3.63×10^{-1}	5.18	
Cu(2)GO cleaned/GC	2.005	6.51×10^{-1}	3.99	8.6
Cu(0.1)PG/GC	0.197	4.23×10^{-2}	6.04	
Cu(1)PG/GC	1.001	3.63×10^{-1}	3.58	
Cu(2)PG/GC	2.258	7.30×10^{-1}	4.00	27.0
Cu(0.1)GC	0.030	4.23×10^{-2}	0.919	
Cu(1)GC	0.121	3.63×10^{-1}	0.433	
Cu(2)GC	0.479	6.39×10^{-1}	0.97	31.2
Cu NPs/GC	0.287	3.46×10^{-1}[c]	1.08	12.0
Cu NPs/GC	0.756	6.92×10^{-1}[c]	1.42	12.0

[a]Cu was loaded onto the GO electrode by electrodeposition from electrolytes spiked with Cu at the indicated concentrations (see text). [b]Already present as an impurity in as-received GO. [c]Mass of Cu nanoparticles loaded on 1 cm^2 of glassy carbon.

DOI: 10.1021/acscatal.5b02399
ACS Catal. 2016, 6, 202−209

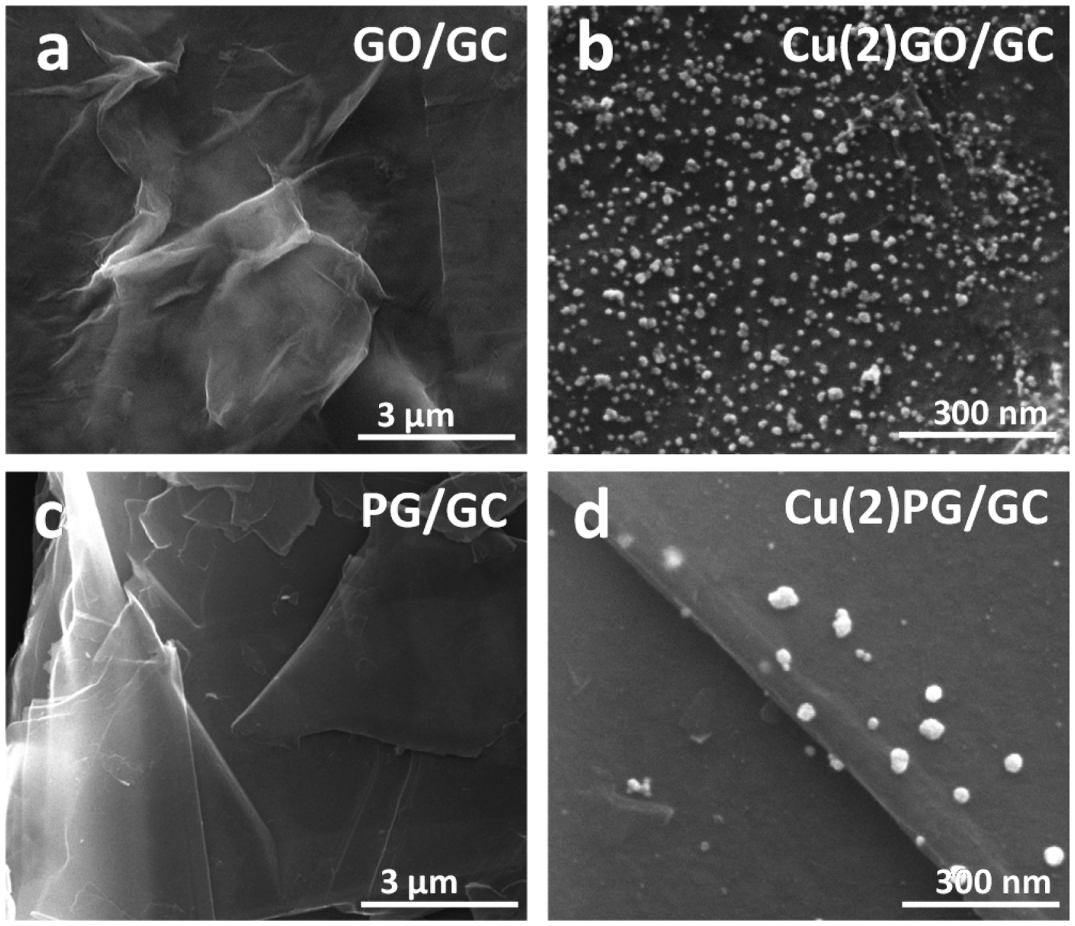

Figure 3. SEM images of GO (a) and PG (c) deposited on glassy carbon. (b) and (d) are higher magnification images after Cu electrodeposition from an electrolyte containing 2 ppm of Cu and 2 h of operation at −1.3 V vs RHE in CO_2-saturated electrolyte. The bright spots are Cu nanoparticles (NPs) with an average size of 8.6 nm on GO (b) and 27.0 nm on PG (d).

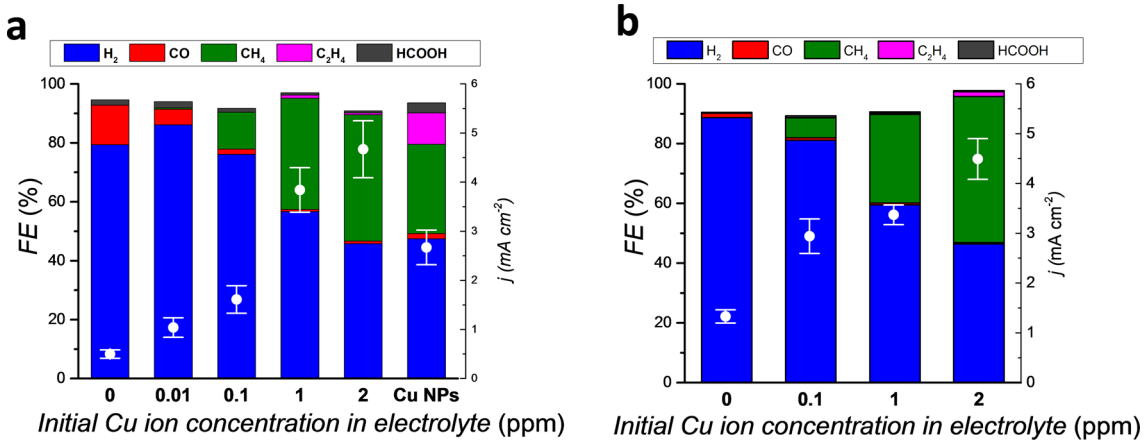

Figure 4. Faradaic efficiencies (FE, shown as bars, left-hand axis) and current densities (open white circles with error bars, right-hand axis) of (a) cleaned graphene oxide (GO) with the indicated concentrations of Cu ion initially "spiked" in the electrolyte and Cu nanoparticles (Cu NPs, 9.69 μg loading) loaded on GC and (b) as-received PG with various concentrations of Cu initially "spiked" in the electrolyte. Electrolysis was carried out at −1.3 V vs RHE in 0.1 M $NaHCO_3$ solution for 2 h. See Tables S11−S14 in the Supporting Information for detailed product distributions.

CNT/GC was not tested, due to difficulties in completely removing metallic impurities from CNTs. Experiments were also conducted with Cu electrodeposited on GC and with Cu nanoparticles dispersed on GC.

The deposition of Cu onto the carbon supports at an applied potential of −1.3 V vs RHE is expected, as the standard potential for reduction of Cu^{2+} to Cu^0 is +0.34 V vs RHE.[35] The maximum amount of Cu that can be deposited is determined from the concentration of copper in the electrolyte and the volume of electrolyte used (0.5 mL) (Table 2). The actual loading of Cu deposited onto each electrode was verified via ICP-MS postelectrolysis (Table S10 in the Supporting Information). By this means, the efficiency of Cu deposition was found to be between 40% and 85% and, in most cases,

DOI: 10.1021/acscatal.5b02399
ACS Catal. 2016, 6, 202−209

between 60% and 85%. For ease of reading, GC, GO/GC, and PG/GC tested in electrolyte containing 0.1 ppm of copper will be termed Cu(0.1)GC, Cu(0.1)GO/GC, and Cu(0.1)PG/GC. A similar notation is used to identify samples produced from electrolyte solutions containing lower and higher concentrations of Cu^{2+}.

SEM images of the morphology of the carbon materials were taken before and after CO_2RR for 2 h with 2 ppm of copper initially in the electrolyte (Figure 3 and Figure S7 in the Supporting Information). These images show that, during the CO2RR experiment, copper is electrodeposited as nanoparticles. The average sizes of the copper nanoparticles are 8.6, 27.0, and 31.2 nm for Cu(2)GO/GC, Cu(2)PG/GC, and Cu(2)GC, respectively. TEM images of Cu(0.1)GO/GC acquired after CO_2RR are shown in Figure S8a in the Supporting Information. The surface of the GO/GC shows no evidence of Cu nanoparticles. TEM inspection of Cu(0.1)GO/GC taken after CO2RR did show Cu nanoparticles. A representative copper nanoparticle and a fast Fourier transform (FFT) of this particle are shown in Figure S8b. The absence of clearly defined lattice fringes in the FFT suggests that the particle is polycrystalline.

The catalytic CO2RR activity of these carbon materials with deposited Cu was tested. Figure 4 shows the product distributions and the measured current densities for CO_2 reduction conducted over Cu(X)GO/GC and Cu(X)PG/GC in electrolytes containing different initial concentrations of Cu, where X is the initial concentration of Cu in the spiked electrolyte. More detailed data for Cu(X)GO/GC, Cu(X)PG/GC, and Cu(X)GC are given in Tables S11−S14 in the Supporting Information. It is apparent that with increasing copper concentration in the electrolyte both the current densities and the FEs for methane increase for both PG and GO. For both Cu(1)GO/GC and Cu(1)PG/GC, the FE for methane reaches about 40%. This FE is comparable to values reported for copper foil, although the Cu foil has a higher current density;[1,9] for Cu(2)GO/GC, the current density is ∼4.6 mA cm^{-2}, which is a factor of 2−3 lower than that for a Cu foil (∼10 mA cm^{-2}) at similar applied potentials.[1,9] The highest selectivity for methane formation is observed on Cu(2)PG/GC and Cu(2)GO/GC. This is particularly interesting in that a direct comparison with GC at identical copper loadings shows much lower activity on the Cu in comparison to GC. For example, the FE for methane only reaches 12.9% for Cu(2)GC in comparison to 43.6% for Cu(2)GO/GC or 38.8% for Cu(2)PG/GC.

To further explore the specific activity of each samples to methane, the mass activities of Cu in Cu(X)GO/GC, Cu(X)PG/GC, and Cu(X)GC were calculated at an applied voltage of −1.3 V (Table 2). The activity of Cu NPs deposited on GC was also calculated at the same voltage for comparison. For further comparison the methane mass activity for as-received GO/GC due to the Cu impurity was calculated and is presented in Table 2. The methane activity per unit mass of Cu of uncleaned GO/GC is as much as 2 orders of magnitude higher than that of any other sample examined. Cu electrodeposited onto acid-washed GO supported on GC (Cu(X)-GO/GC) is comparable to that of Cu(X)PG/GC. While some differences in the methane activity per gram of Cu are observed with Cu loading, these variations are not systematic. In all cases the activity of these samples is about an order of magnitude lower than that for uncleaned GO/GC. An additional observation is that the activity of Cu electrodeposited onto GC is ∼4−5 times lower than that of Cu(X)GO/GC or Cu(X)PG/GC.

It is interesting to consider why Cu electrodeposited on GO/GC and PG/GC exhibit significantly higher methane activity per gram of Cu than Cu electrodeposited on GC or premade Cu NP dispersed on GC. Some insights into this question can be drawn from a theoretical investigation of the CO2RR occurring on copper nanoclusters (∼0.9 nm in diameter) supported on graphene at defect sites.[36,37] This work indicates that the activation energy for the protonation of adsorbed CO to form adsorbed CHO, the elementary step believed to be the rate-limiting step for CH_4 formation, is ∼30% of that for the same reaction occurring on a Cu (111) surface. This effect is attributed to greater orbital hybridization of the copper nanoparticles on graphene with the adsorbed CHO intermediate in comparison to the Cu(111) surface, leading to greater stabilization of the intermediate. The authors also show that the energy barrier for the HER on these graphene-supported copper nanoparticles is slightly higher than that determined for the HER occurring on a Cu(111) surface, indicating a slight suppression of the HER. We, therefore, propose that the Cu impurities present on as-received GO may be segregated preferentially at defects on the GO planes and that Cu associated with such sites may be exceptionally active. By extension, we propose that electrodeposition of Cu onto acid-washed GO/GC or PG/GC places a significant fraction of the Cu onto defect sites present in either acid-washed GO or as-received PG. If this reasoning is correct, then the lower activity of Cu electrodeposited on GC may be a consequence of a level of defects on the GC being lower than that on GO or PG.

CONCLUSIONS

The studies reported here demonstrate that as-received carbon supports can contain significant concentrations of metallic impurities which are active for the CO2RR. Of particular note is GO, which can contain significant concentrations of Cu. The presence of Cu in as-received GO explains why this material is active for the formation of methane during the electroreduction of CO_2. Nearly all of the catalytically relevant metallic impurities can be removed from GO by washing in ultrapure nitric acid. When this is done, the electrochemical activity for both GO and the other carbon supports tested decreases and the activity for methane formation on GO disappears. Furthermore, Cu can be added back to the now clean carbon supports via electrochemical deposition. When this is done, the activity for methane formation returns and increases with an increase in the amount of Cu deposited. The activity per mass of Cu is ∼4−5 times higher when Cu is deposited onto GO or PC dispersed on GC in comparison to Cu deposited onto GC. The higher electrochemical activity of Cu electrodeposited on to GO/GC or PG/GC is attributed to the preferential deposition of Cu NPs at defects present on the graphene layers of GO and PG. This effect is thought to be more extreme in the as-received GO/GC, which shows the Cu highest mass activity for methane production. This work suggests that a highly active catalyst for methane formation via the CO2RR can be created by the introduction of defects into graphene layers, onto which Cu can then be electrodeposited and exhibit enhanced activity.

DOI: 10.1021/acscatal.5b02399
ACS Catal. 2016, 6, 202−209

■ ASSOCIATED CONTENT

Supporting Information

The Supporting Information is available free of charge on the ACS Publications website at DOI: 10.1021/acscatal.5b02399.

X-ray photoelectron spectroscopy (XPS), specific surface area measurements, electroactive surface area (EASA), efficacy of the high-purity nitric acid washing procedure, comparison of impurity concentrations in graphene oxide from four sources, washing carbon materials with reagent grade nitric acid, supplemental Cu loading and Faradaic efficiency, scanning electron microscopy, transmission electron microscopy, and long-duration CO2RR testing (PDF)

■ AUTHOR INFORMATION

Corresponding Authors

*E-mail for A.T.B.: alexbell@berkeley.edu

*E-mail for J.W.A.: jwager@lbl.gov.

Author Contributions

[#]These authors (Y.L. and Y.K.) contributed equally to this work.

Notes

The authors declare no competing financial interest.

■ ACKNOWLEDGMENTS

This material is based upon work performed by the Joint Center for Artificial Photosynthesis, a DOE Energy Innovation Hub, supported through the Office of Science of the U.S. Department of Energy under Award Number DE-SC0004993. The design, construction, and operation of the electrochemical cell were supported by the California Energy Commission under agreement 500-11-023. Y.L. acknowledges the support of an A*STAR National Science Scholarship. We thank Li Yang from Berkeley Lab Earth Sciences Division for technical assistance with the ICP-MS analysis.

■ REFERENCES

(1) Hori, Y. In *Modern Aspects of Electrochemistry*; Vayenas, C. G., White, R. E., Gamboa-Aldeco, M. E., Eds.; Springer: New York, 2008; pp 89−189.

(2) Graves, C.; Ebbesen, S. D.; Mogensen, M.; Lackner, K. S. *Renewable Sustainable Energy Rev.* **2011**, *15*, 1−23.

(3) Kim, D.; Sakimoto, K. K.; Hong, D.; Yang, P. *Angew. Chem., Int. Ed.* **2015**, *54*, 3259−3266.

(4) Torella, J. P.; Gagliardi, C. J.; Chen, J. S.; Bediako, D. K.; Colón, B.; Way, J. C.; Silver, P. A.; Nocera, D. G. *Proc. Natl. Acad. Sci. U. S. A.* **2015**, *112*, 2337−2342.

(5) Liu, C.; Gallagher, J. J.; Sakimoto, K. K.; Nichols, E. M.; Chang, C. J.; Chang, M. C. Y.; Yang, P. *Nano Lett.* **2015**, *15*, 3634−3639.

(6) Gattrell, M.; Gupta, N.; Co, A. *J. Electroanal. Chem.* **2006**, *594*, 1−19.

(7) Jones, J.-P.; Prakash, G. K. S.; Olah, G. A. *Isr. J. Chem.* **2014**, *54*, 1451−1466.

(8) Delacourt, C.; Newman, J. *J. Electrochem. Soc.* **2010**, *157*, B1911−B1926.

(9) Kuhl, K. P.; Cave, E. R.; Abram, D. N.; Jaramillo, T. F. *Energy Environ. Sci.* **2012**, *5*, 7050−7059.

(10) Qiao, J.; Liu, Y.; Hong, F.; Zhang, J. *Chem. Soc. Rev.* **2014**, *43*, 631−675.

(11) Kim, D.; Resasco, J.; Yu, Y.; Asiri, A. M.; Yang, P. *Nat. Commun.* **2014**, *5*, 4948.

(12) Lu, Q.; Rosen, J.; Jiao, F. *ChemCatChem* **2015**, *7*, 38−47.

(13) Peterson, A. A.; Abild-Pedersen, F.; Studt, F.; Rossmeisl, J.; Nørskov, J. K. *Energy Environ. Sci.* **2010**, *3*, 1311−1315.

(14) Peterson, A. A.; Nørskov, J. K. *J. Phys. Chem. Lett.* **2012**, *3*, 251−258.

(15) Baturina, O. A.; Lu, Q.; Padilla, M. A.; Xin, L.; Li, W.; Serov, A.; Artyushkova, K.; Atanassov, P.; Xu, F.; Epshteyn, A.; Brintlinger, T.; Schuette, M.; Collins, G. E. *ACS Catal.* **2014**, *4*, 3682−3695.

(16) Kumar, B.; Asadi, M.; Pisasale, D.; Sinha-Ray, S.; Rosen, B. A.; Haasch, R.; Abiade, J.; Yarin, A. L.; Salehi-Khojin, A. *Nat. Commun.* **2013**, *4*, 2819.

(17) Nakata, K.; Ozaki, T.; Terashima, C.; Fujishima, A.; Einaga, Y. *Angew. Chem.* **2014**, *126*, 890−893.

(18) Zhang, S.; Kang, P.; Ubnoske, S.; Brennaman, M. K.; Song, N.; House, R. L.; Glass, J. T.; Meyer, T. J. *J. Am. Chem. Soc.* **2014**, *136*, 7845−7848.

(19) Wu, J.; Yadav, R. M.; Liu, M.; Sharma, P. P.; Tiwary, C. S.; Ma, L.; Zou, X.; Zhou, X.-D.; Yakobson, B. I.; Lou, J.; Ajayan, P. M. *ACS Nano* **2015**, *9*, 5364−5371.

(20) Banks, C. E.; Crossley, A.; Salter, C.; Wilkins, S. J.; Compton, R. G. *Angew. Chem., Int. Ed.* **2006**, *45*, 2533−2537.

(21) Pumera, M.; Iwai, H. *J. Phys. Chem. C* **2009**, *113*, 4401−4405.

(22) Pumera, M. *Langmuir* **2007**, *23*, 6453−6458.

(23) Anik, Ü.; Çevik, S.; Pumera, M. *Nanoscale Res. Lett.* **2010**, *5*, 846−852.

(24) Ambrosi, A.; Chee, S. Y.; Khezri, B.; Webster, R. D.; Sofer, Z.; Pumera, M. *Angew. Chem., Int. Ed.* **2012**, *51*, 500−503.

(25) Ambrosi, A.; Chua, C. K.; Khezri, B.; Sofer, Z.; Webster, R. D.; Pumera, M. *Proc. Natl. Acad. Sci. U. S. A.* **2012**, *109*, 12899−12904.

(26) Wong, C. H. A.; Sofer, Z.; Kubešová, M.; Kučera, J.; Matějková, S.; Pumera, M. *Proc. Natl. Acad. Sci. U. S. A.* **2014**, *111*, 13774−13779.

(27) Wuttig, A.; Surendranath, Y. *ACS Catal.* **2015**, *5*, 4479−4484.

(28) Dong, G.; Fang, M.; Wang, H.; Yip, S.; Cheung, H.-Y.; Wang, F.; Wong, C.-Y.; Chu, S. T.; Ho, J. C. *J. Mater. Chem. A* **2015**, *3*, 13080−13086.

(29) Uk Son, S.; Kyu Park, I.; Park, J.; Hyeon, T. *Chem. Commun.* **2004**, 778−779.

(30) Machado, S. A. S.; Avaca, L. A. *Electrochim. Acta* **1994**, *39*, 1385−1391.

(31) Zou, X.; Zhang, Y. *Chem. Soc. Rev.* **2015**, *44*, 5148−5180.

(32) Kuhl, K. P.; Hatsukade, T.; Cave, E. R.; Abram, D. N.; Kibsgaard, J.; Jaramillo, T. F. *J. Am. Chem. Soc.* **2014**, *136*, 14107−14113.

(33) Hara, K.; Kudo, A.; Sakata, T. *J. Electroanal. Chem.* **1995**, *391*, 141−147.

(34) Azuma, M. *J. Electrochem. Soc.* **1990**, *137*, 1772−1778.

(35) Bard, A. J.; Faulkner, L. R. *Electrochemical Methods: Fundamentals and Applications*, 2nd ed.; Wiley: New York, 2001; p 808.

(36) Lim, D.-H.; Jo, J. H.; Shin, D. Y.; Wilcox, J.; Ham, H. C.; Nam, S. W. *Nanoscale* **2014**, *6*, 5087−5092.

(37) Liu, C.; He, H.; Zapol, P.; Curtiss, L. A. *Phys. Chem. Chem. Phys.* **2014**, *16*, 26584−26599.

DOI: 10.1021/acscatal.5b02399
ACS Catal. 2016, 6, 202−209